SEPARATING THE X-RAY EMISSIONS OF UV CETI A AND B WITH *CHANDRA*

MARC AUDARD,[1] MANUEL GÜDEL,[2] AND STEPHEN L. SKINNER[3]

ABSTRACT

We present the first spatially separated X-ray observation of the active UV Ceti binary with *Chandra*, providing important new information on the relative X-ray activity levels of its nearly identical dM5.5e components. The two components had similar X-ray luminosities during low-level periods, and emission measure loci derived from Low Energy Transmission Grating spectra reveal similar coronal temperatures (3–6 MK). However, the B component showed a higher degree of variability, resulting in a higher average X-ray luminosity than that of UV Cet A. We discuss possible causes of this enhanced activity in UV Cet B.

Subject headings: binaries: visual — stars: coronae — stars: flare — stars: individual (UV Ceti) — stars: late-type — X-rays: stars

1. INTRODUCTION

The nearby ($d = 2.7$ pc) binary UV Ceti (GJ 65 AB; L726-8 AB) is composed of two dM5.5e stars with similar masses and radii ($M \approx 0.1\ M_{\odot}$, $R \approx 0.15\ R_{\odot}$) in a highly eccentric orbit with a period of 26.5 yr and a semimajor axis of $\approx 2''$ (5.06 AU; Worley & Behall 1973; Geyer, Harrington, & Worley 1988). UV Cet is the prototype of flare stars and has been extensively studied from radio to X-rays (e.g., de Jager et al. 1989; Stepanov et al. 1995; Güdel et al. 1996). Previous X-ray observatories could not separate the components (Pallavicini, Tagliaferri, & Stella 1990; Schmitt, Haisch, & Barwig 1993). However, high angular resolution radio observations have resolved the binary into its components and show that their radio emissions significantly differ: UV Cet B flares more frequently than UV Cet A and is also an order of magnitude brighter in its steady radio emission (e.g., Gary & Linsky 1981; Gary, Linsky, & Dulk 1982; Kundu et al. 1987; Jackson, Kundu, & White 1987; Kundu et al. 1988; Jackson, Kundu, & White 1989; Benz, Conway, & Güdel 1998). The different radio behavior of UV Cet A/B raises the obvious question of whether the X-ray properties of the two components are also different. Although previous X-ray observatories lacked sufficient angular resolution to answer this question, it can now be addressed with *Chandra*. We present here the first spatially separated X-ray observation of UV Cet A/B. Light curves and spectral emission lines were extracted for both components. A detailed analysis of the *Chandra* data and of *XMM-Newton* and VLA observations of UV Cet will be presented in a forthcoming paper.

2. OBSERVATIONS

The *Chandra* X-ray Observatory observed the UV Cet binary for 75 ks from 2001 November 26 at 20:55:39 UT to 2001 November 27 at 18:09:27 UT, with the Low Energy Transmission Grating Spectrometer (LETGS) inserted. This configuration provides grating spectra from 1.7 to 177 Å with a constant resolution of $\Delta\lambda \approx 0.05$ Å (FWHM). The positive- and negative-order spectra are dispersed on the High-Resolution Camera (HRC-S) on each side of the focal aim point, and the latter provides a direct zeroth-order image of the target in the energy range 0.08–10 keV with an angular resolution of $0''.4$ (FWHM). The HRC " pixel " size is $0''.13175$. Further details on the instruments can be found in the *Chandra* Proposers' Observatory Guide.[4]

We reduced level 2 files provided by the *Chandra* X-ray Center, following recommended procedures with the CIAO 2.2.1 software. The binary was aligned almost along the dispersion axis and was separated in the grating spectra by about 80 mÅ. This way, in the negative-order spectrum emission lines of UV Cet A were shifted to shorter wavelengths relative to UV Cet B, whereas they were shifted to longer wavelengths in the positive order.

3. SEPARATING UV CETI A AND B

Figure 1 shows the zeroth-order image of the binary; the astrometry is expected to be accurate within $1''$. We used a sliding cell source detection algorithm with a fixed cell size of 6 pixels ($0''.79$). The components were separated by $1''.54$, with UV Cet B lying at a position angle of $117°.05$ relative to A. At the epoch of our observation, the orbital solution of Geyer et al. (1988) gives a separation of $d = 1''.45$ and a position angle of $117°.1$, whereas the solution of Worley & Behall (1973) gives $d = 1''.54$ and an angle of $117°.3$. Our X-ray positions are therefore in excellent agreement with the expected optical positions.

4. LIGHT CURVES

We extracted zeroth-order light curves for each component by using circular regions with radii of 5.5 pixels ($\approx 0''.72$) and applied dead-time corrections. The background contribution was estimated from nearby regions and was negligible ($\approx 5.6 \times 10^{-5}$ counts s^{-1}, scaled to the source extraction region).

Figure 2 shows the X-ray light curves for both components. Obviously, UV Cet B was highly variable and showed at least five large flares, while UV Cet A showed only a

[1] Columbia Astrophysics Laboratory, Mail Code 5247, 550 West 120th Street, New York, NY 10027; audard@astro.columbia.edu.

[2] Paul Scherrer Institut, Villigen and Würenlingen, 5232 Villigen PSI, Switzerland; guedel@astro.phys.ethz.ch.

[3] Center for Astrophysics and Space Astronomy, University of Colorado, Boulder, CO 80309-0389; skinners@casa.colorado.edu.
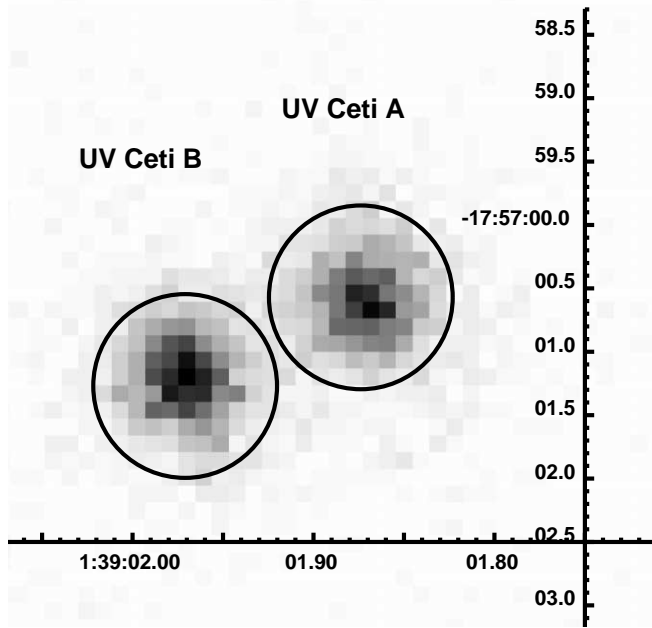
[4] See http://cxc.harvard.edu/proposer/POG.

FIG. 1.—Zeroth-order image of the low-level X-ray emissions of UV Cet A and B. Circles of 5.5 pixels (0″.72) are centered on the positions of each component. The axes give the J2000.0 coordinates in right ascension (*horizontal*) and declination (*vertical*). The coordinates for UV Cet A are $\alpha = 1^h39^m01^s87$ and $\delta = -17°57'00″.6$, whereas they are $\alpha = 1^h39^m01^s97$ and $\delta = -17°57'01″.3$ for UV Cet B.

$[L_X \approx (1.0–1.2) \times 10^{-27}$ ergs s^{-1} for each component, 0.1–10 keV, based on a simulation of a 0.34 keV (see § 5) coronal plasma with solar abundances in the Portable, Interactive Multi-Mission Simulator (PIMMS); Mukai 1993].

UV Cet B displayed two types of flares: the first type is characterized by a slow increase and a slow decay, with similar timescales. The second flare type is reminiscent of "impulsive" solar flares, with a rapid rise and a slower decay. Both flare types, however, share similar total durations of $\approx$2000–3000 s. The peak count rate of the giant flare in UV Cet B is about a factor of 100 over the low-level count rate ($L_{X,peak} \approx 2 \times 10^{29}$ ergs s^{-1} for a 1.37 keV plasma in PIMMS); the flare has a very short rise time of 80 s and returns to the preflare level after $\approx$2300 s (see Fig. 2, *inset*). A secondary peak occurs during the decay phase of the first flare, perhaps indicating the occurrence of a second flare.

5. SPECTRA

We present in this section a discussion of the *Chandra* LETGS spectra of UV Cet A and B. In this paper, our analysis focuses on the low-level emission (50.8 ks); however, we do note that emission lines from higher ionization stages of Fe (e.g., Fe XXIII and Fe XXIV in the 10–12 Å range) were seen during flares. The selected time intervals for the low-level emission are shown in Figure 2 (*top*). Figure 3 shows the full *Chandra* positive- and negative-order spectra during the low-level emission. Since the latter is faint (a total of 0.11 counts s^{-1} in the dispersed spectra), only a few bright emission lines have been positively detected. The low-level X-ray spectra of UV Cet A and B are similar. They show the strongest emission in the O VIII Lyα line. Emission lines from Fe XVII, Ne IX, Ne X, C VI, N VII, and O VII are also detected below 40 Å. The range of temperatures over which these lines form indicates that there is significant emission
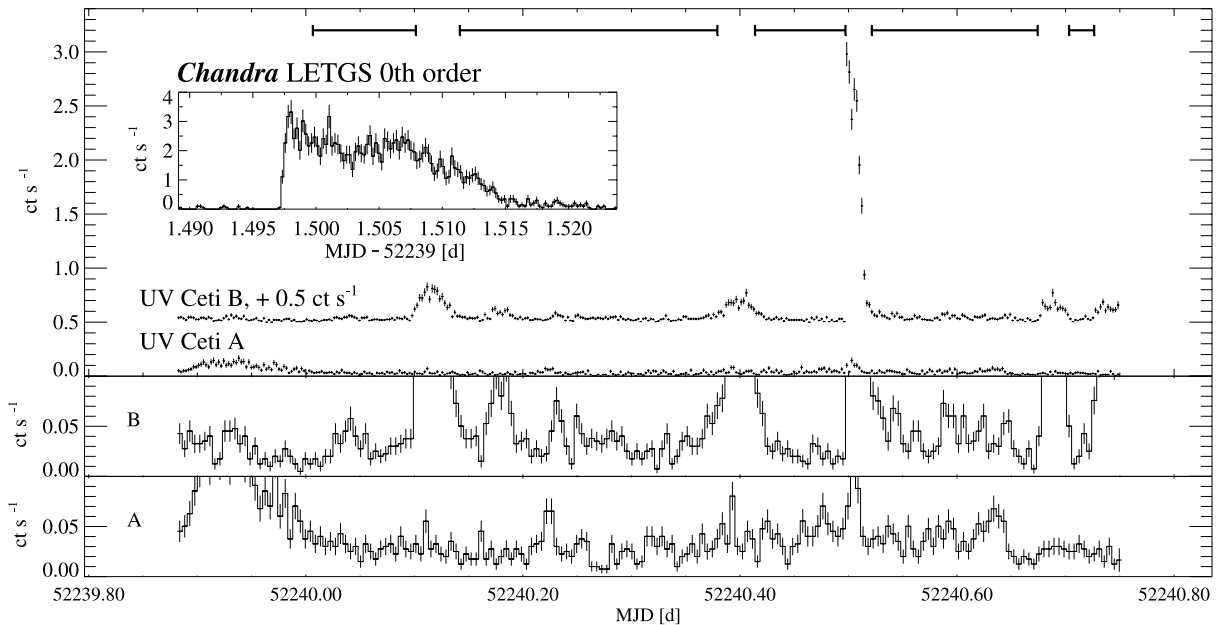
gradual rise and fall at the start of the observation. The small flare in UV Cet A occurring simultaneously with the large flare in UV Cet B is an artifact due to flux contamination from component B to component A. The two stars had a similar low-level X-ray count rate (excluding the five large flares; see Fig. 2), around 0.025–0.03 counts s^{-1}

FIG. 2.—Zeroth-order HRC-S/LETG light curves of UV Cet A and B (0.1–10 keV). *Top*: Light curves shown here with a bin size of 200 s. The curve for UV Cet B shifted by +0.5 counts s^{-1} for clarity. The five time spans at the top represent the selected time intervals for the low-level LETGS spectra shown in Fig. 3. *Inset:* Extract of the large flare on UV Cet B for a bin size of 20 s. The flare emission increased by a factor of about 100 above the low-level emission. The flare rise time is $\approx$80 s, whereas the count rate returns to the preflare level after $\approx$2300 s. *Middle and bottom*: Low-level X-ray emission of UV Cet B (*middle*) and UV Cet A (*bottom*), respectively. The bin size is 400 s.
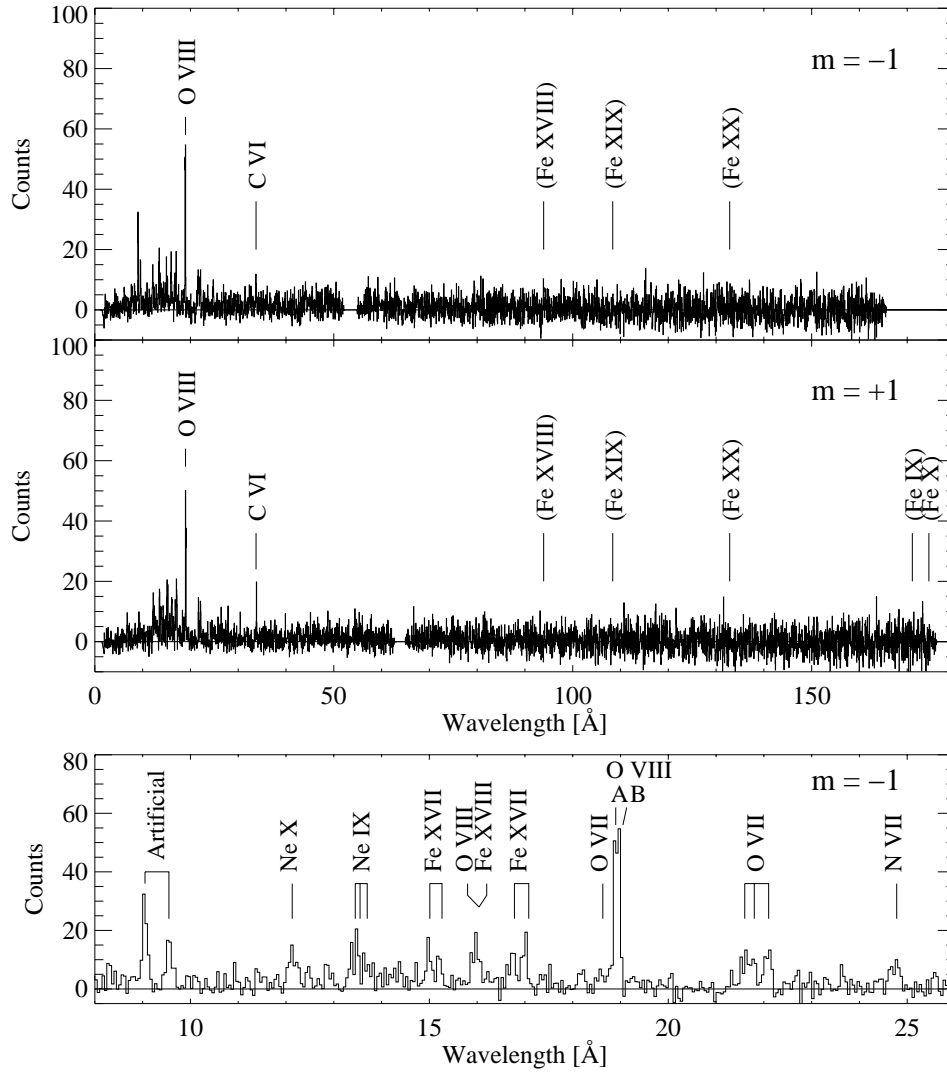
Fig. 3.—*Top and middle:* Low-level *Chandra* LETGS spectra in the negative (*top*) and positive (*middle*) orders for an exposure time of 50.8 ks and a bin size of 50 mÅ. With such a bin size, the contributions from each source are averaged. We indicated in parentheses the expected location of bright lines formed at high temperature (Fe xviii through Fe xx) and at low temperature (Fe ix and Fe x) in the long-wavelength range. *Bottom*: Extract of the negative-order spectrum between 8 and 26 Å. Two emission features at 9.04 and 9.55 Å appear in the negative-order spectrum and have been identified as zeroth-order contaminations from faint sources that fell by chance on the dispersed spectrum.

measure (EM) in the range $T = 3$–6 MK, which is confirmed by electron temperature diagnostics such as line ratios. Reliable density measurements could not be obtained because of low fluxes in the closely spaced helium-like triplets and line blending (see, e.g., Fig. 4*b* and Fig. 4*d*). At longer wavelengths (≥ 40 Å), the signal-to-noise ratio was insufficient to significantly detect emission lines. We derived upper limits to fluxes of Fe L shell lines with typical large emissivities, such as Fe xviii $\lambda 93.92$, Fe xix $\lambda 108.37$, Fe xxi $\lambda 128.73$, Fe xx/Fe xxiii $\lambda 132.85$, Fe ix $\lambda 171.07$, and Fe x $\lambda 174.53$. The absence of detectable emission from these lines suggests that there is no significant EM at high ($T \geq 6$ MK) or low ($T \leq 2$ MK) temperatures.

We fitted the positive- and negative-order spectra simultaneously with two monochromatic emission lines per feature (for UV Cet A and B), folded through the *Chandra* line response function. In the negative-order spectrum, the model line wavelengths were shifted by -12 mÅ to account for the wavelength discrepancy between the positive- and negative-order spectra with CIAO 2.2.1. The emission lines

from UV Cet A and B were separated by a fixed 80 mÅ. First-order grating response matrices from 2002 July as provided by the LETGS calibration team were used.[5] Line emissivities from APEC 1.2 (Smith et al. 2001) were used to calculate the EM loci curves. We assumed that the coronal abundances in UV Cet A and B were identical to the solar photospheric abundances (Anders & Grevesse 1989). The line fluxes were not corrected for interstellar absorption, since it is very small ($N_{\rm H} \approx 6 \times 10^{17}$ cm^{-2} based on the canonical interstellar density $n_{\rm H} \approx 0.07$ cm^{-3}; Paresce 1984), even at the long-wavelength end of the LETGS (8% absorption at 170 Å). We provide EM loci of UV Cet A and B in Figure 5; EM loci of detected Fe lines (*solid curves*) and of detected other elements (*dotted curves*) are shown with 68% confidence ranges at the maximum formation temperatures ($T_{\rm max}$), suggesting that Ne and O are overabundant relative
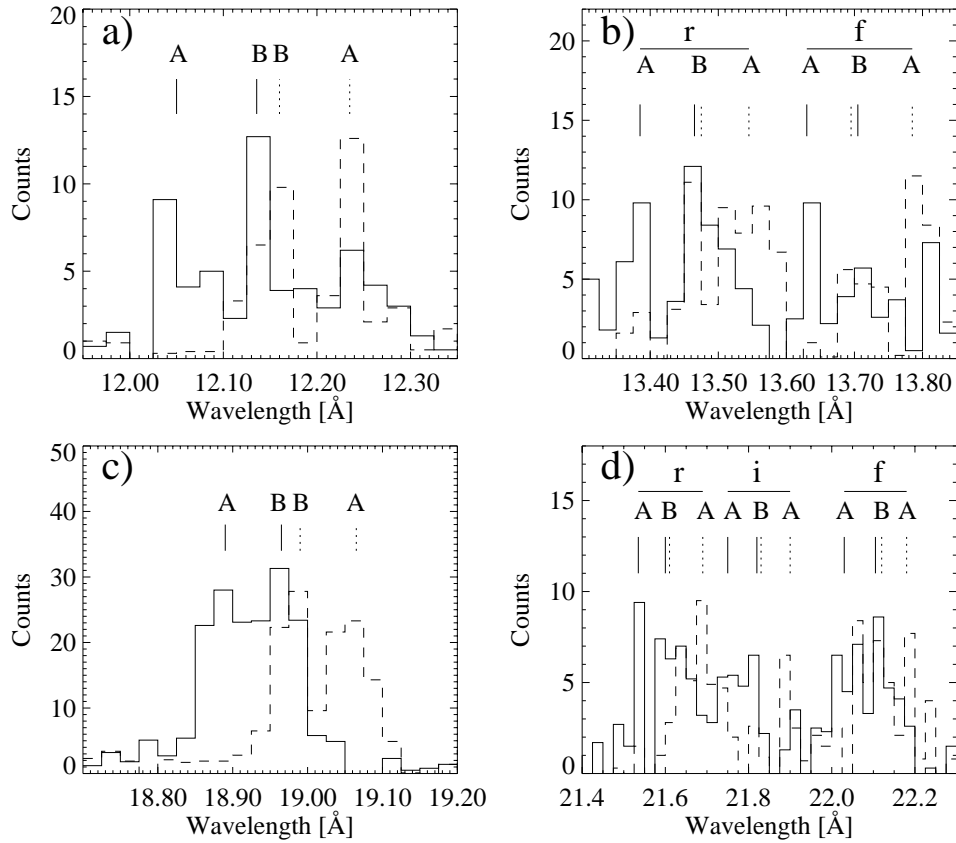
[5] See
http://cxc.harvard.edu/cal/Links/Letg/User/Hrc_QE/ea_index.html.

Fig. 4.—Extract from low-level *Chandra* spectra in the region of (*a*) Ne x Lyα, (*b*) Ne ix Heα, (*c*) O viii Lyα, and (*d*) O vii Heα for a bin size of 25 mÅ and an exposure time of 50.8 ks. The solid line shows the negative-order spectrum, whereas the dashed line stands for the positive-order spectrum. The wavelength discrepancy originates from the inaccuracy of the relative wavelength calibration between the negative- and positive-order LETGS spectra with CIAO 2.2.1. In each panel, the emission of each binary component has been labeled. In (*b*), we show only the resonance (*r*) and forbidden (*f*) lines, whereas in (*d*) the intercombination (*i*) line is also shown.
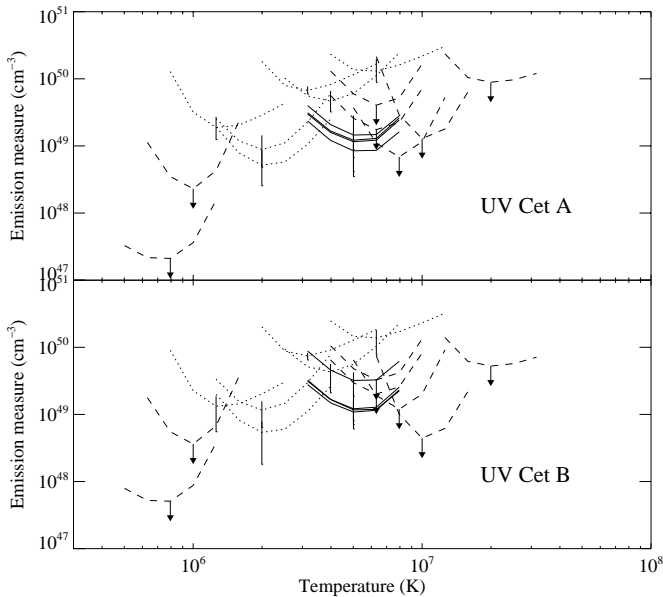

Fig. 5.—For UV Cet A and B, emission loci for detected Fe lines (with 68% confidence ranges shown as vertical ranges; *solid curves*), for detected lines from other ions (O viii, O vii, Ne x, Ne ix, and C vi, with 68% confidence ranges shown as vertical ranges; *dotted curves*), and for the upper limits (from 90% confidence ranges; *dashed curves*) of undetected Fe lines. Emissivities from APEC 1.2 were used assuming solar photospheric abundances (Anders & Grevesse 1989).

to Fe. Upper limits (90% confidence ranges) for the EM loci of undetected Fe lines (*dashed curves*) are also shown with arrows at T_{max}.

We have checked the consistency of our upper limits with the archival *Extreme Ultraviolet Explorer* (*EUVE*) data of UV Cet. Since this paper aims at presenting the new *Chandra* results, we present here only a summary of the *EUVE* analysis. The UV Cet binary was observed during a time span of 885 ks, with an effective exposure of about 230 ks. Its deep survey (DS; 65–190 Å) light curve displayed strong variability with several short flarelike events. We extracted the short-wavelength (SW; 70–190 Å) spectrum during the low-level emission (DS count rates lower than 0.1 counts s⁻¹; exposure of 188 ks) and compared the line fluxes with those in the *Chandra* LETGS spectrum. We emphasize that *EUVE* could not separate the binary spatially and spectroscopically. Only two lines were detected, the Fe xx/ Fe xxiii λ132.85 blend and the Fe xviii λ93.92 line; their measured fluxes were $(8.1 \pm 5.0) \times 10^{-5}$ and $(5.9 \pm 3.2) \times 10^{-5}$ photons cm⁻² s⁻¹, respectively. The sum of the upper limits for UV Cet A/B obtained from the LETGS (at 132.85 Å, $\leq 6.2 \times 10^{-5}$ and $\leq 9.1 \times 10^{-5}$ photons cm⁻² s⁻¹; at 93.92 Å, $\leq 5.4 \times 10^{-5}$ and $\leq 6.2 \times 10^{-5}$ photons cm⁻² s⁻¹, for UV Cet A and B, respectively) is compatible with the measured fluxes in *EUVE* SW. The other Fe L shell lines that are formed at high or low temperature (see previous paragraph) remain undetected by *EUVE*, and their upper limits are also consistent with our *Chandra* upper limits.

6. DISCUSSION AND CONCLUSIONS

Numerous radio observations of the UV Cet binary system have shown that the coronae of both components differ significantly. The nonflaring radio emission of the primary is much weaker than that of the secondary and often remains undetected (e.g., Gary et al. 1982; Kundu et al. 1987). Their flares also are different: on UV Cet A, flares are often highly circularly polarized, thus suggesting some coherent emission mechanism (Gary et al. 1982; Benz et al. 1998; Bingham, Cairns, & Kellett 2001), whereas flares in UV Cet B often show only weak or moderate polarizations consistent with gyrosynchrotron emission (e.g., Jackson et al. 1987; Güdel et al. 1996) and occur more frequently than flares in the primary.

The contrasting behavior in the radio is peculiar since the two stars are otherwise thought to be very similar, with almost identical masses and radii. A study of their spatially separated X-ray emissions thus promises to uncover differences in the coronal energy release behavior of the two stars. UV Cet A did not display any strong X-ray variability, while UV Cet B was on average twice as luminous as the primary, essentially because it displayed a higher flare rate (Fig. 2, *top*). The radio emission is due to the production of high-energy electrons during the flare process. Gyrosynchrotron emission under solar-like conditions would decay rapidly (within minutes) because of radiation and collisional losses. However, if extended, weak magnetic fields B were present, then part of the relativistic electron population produced during the detected large X-ray flares could be efficiently trapped for durations τ much longer than the characteristic time between large flares since $\tau \propto B^{-3/2}$ for synchrotron losses. Spatially resolved VLBA observations support such a model for UV Cet B (whereas no extended structure was identified in the primary). Benz et al. (1998) inferred magnetospheric structures around UV Cet B several times larger than the star, and from the decay time of a gradual flare ($\tau \approx 6500$ s) they inferred magnetic field strengths of only a few tens of gauss. Based on this observation, Kellett et al. (2002) further proposed a magnetic trap model that would at the same time explain the steady radio and X-ray emission.

In contrast to the quasi-steady radio emission of each component, the quasi-steady X-ray count rates of the two components are similar. A closer look at the *Chandra* low-level light curve of UV Cet B (Fig. 2, *middle*) shows that its "quiescent" emission is in fact flickering and is composed of numerous temporally resolved flares, with a possible quasi-steady emission not exceeding 0.01 counts s^{-1} or 30% of the average low-level emission. It may well be that the entire X-ray emission is a superposition of the detected flare decays, including very small events. This could be similar for the X-ray emission of UV Cet A (Fig. 2, *bottom*). Accelerated electrons from these flares can further add to the quasi-steady radio emission, but they are particularly well trapped in the extended magnetosphere of UV Cet B. *XMM-Newton* data of the dM5.5e star Proxima Centauri have yielded similar results; its quiescent X-ray emission was temporally resolved into a continual sequence of weak flares (Güdel et al. 2002). These results provide strong support for the hypothesis that low-energy flares contribute significantly to the coronal heating in stars (Audard et al. 2000; Kashyap et al. 2002; Güdel et al. 2003). In the Sun, flares with small energies contribute a significant amount to the total coronal heating (e.g., Krucker & Benz 1998; Parnell & Jupp 2000).

In conclusion, the radio and X-ray behaviors of UV Cet A and B are strikingly different. VLBA measurements have revealed an extended magnetosphere around UV Cet B only, and *Chandra* shows that the B component displays a harder distribution of X-ray flares. Such flares may repeatedly produce and trap electrons in the extended magnetosphere at a rate sufficient to sustain the quasi-steady radio emission. Given the similar masses and spectral types of the binary components, it is yet unclear why their coronal behavior should differ. Stellar rotation may play an important role, since coronal activity is roughly proportional to the rotation rate. Infrared spectroscopy has recently shown that UV Cet A rotates relatively fast ($v \sin i = 58$ km s^{-1}; Hinkle et al. 2003), but to our knowledge no measurement is yet available for UV Cet B. The physical causes responsible for the disparate coronal behaviors of these two stars remain yet unexplained; however, the answer to this question may provide important information on the generation and sustainment of magnetic fields in late-type stars.

REFERENCES

Anders, E., & Grevesse, N. 1989, Geochim. Cosmoschim. Acta, 53, 197
Audard, M., Güdel, M., Drake, J. J., & Kashyap, V. L. 2000, ApJ, 541, 396
Benz, A. O., Conway, J., & Güdel, M. 1998, A&A, 331, 596
Bingham, R., Cairns, R. A., & Kellett, B. J. 2001, A&A, 370, 1000
de Jager, C., et al. 1989, A&A, 211, 157
Gary, D. E., & Linsky, J. L. 1981, ApJ, 250, 284
Gary, D. E., Linsky, J. L., & Dulk, G. A. 1982, ApJ, 263, L79
Geyer, D. W., Harrington, R. S., & Worley, C. E. 1988, AJ, 95, 1841
Güdel, M., Audard, M., Kashyap, V. L., Drake, J. J., & Guinan, E. F. 2003, ApJ, 582, 423
Güdel, M., Audard, M., Skinner, S. L., & Horvath, M. 2002, ApJ, 580, L73
Güdel, M., Benz, A. O., Schmitt, J. H. M. M., & Skinner, S. L. 1996, ApJ, 471, 1002
Hinkle, K. H., Valenti, J., Wallace, L., & Tsuji, T. 2003, BAAS, 34(144.01)
Jackson, P. D., Kundu, M. R., & White, S. M. 1987, ApJ, 316, L85
———. 1989, A&A, 210, 284
Kashyap, V. L., Drake, J. J., Güdel, M., & Audard, M. 2002, ApJ, 580, 1118

Kellett, B. J., Bingham, R., Cairns, R. A., & Tsikoudi, V. 2002, MNRAS, 329, 102
Krucker, S., & Benz, A. O. 1998, ApJ, 501, L213
Kundu, M. R., Jackson, P. D., White, S. M., & Melozzi, M. 1987, ApJ, 312, 822
Kundu, M. R., Pallavicini, R., White, S. M., & Jackson, P. D. 1988, A&A, 195, 159
Mukai, K. 1993, Legacy, 3, 21
Pallavicini, R., Tagliaferri, G., & Stella, L. 1990, A&A, 228, 403
Paresce, F. 1984, AJ, 89, 1022
Parnell, C. E., & Jupp, P. E. 2000, ApJ, 529, 554
Schmitt, J. H. M. M., Haisch, B., & Barwig, H. 1993, ApJ, 419, L81
Smith, R. K., Brickhouse, N. S., Liedahl, D. A., & Raymond, J. C. 2001, ApJ, 556, L91
Stepanov, A. V., Fürst, E., Krüger, A., Hildenbrandt, J., Barwig, H., & Schmitt, J. H. M. M. 1995, A&A, 299, 739
Worley, C. E., & Behall, A. L. 1973, AJ, 78, 650